Journal of Molecular Modeling (2023) 29:119
https://doi.org/10.1007/s00894-023-05526-3

ORIGINAL PAPER

Transition metal (X = Mn, Fe, Co, Ni, Cu, Zn)-doped graphene as gas sensor for CO_2 and NO_2 detection: a molecular modeling framework by DFT perspective

Fatemeh Mollaamin[1] · **Majid Monajjemi**[2]

Received: 30 January 2023 / Accepted: 22 March 2023 / Published online: 29 March 2023

Abstract

Context In this research, CO_2 and NO_2 adsorption on doped nanographene (NG) sheets with transition metals (Fe, Ni, Zn) and (Mn, Co, Cu), respectively, have been applied for scavenging of these toxic gases as the environmental pollutants. The values of changes of atomic charge density have illustrated a more significant charge transfer for Ni-doped C-NG through CO_2 adsorption and a more remarkable charge transfer for Co-doped C-NG through NO_2 adsorption. The data of NMR spectroscopy has depicted several fluctuations around the graph of Zn-doped on the nanographene surface. The thermodynamic results from IR spectroscopy have indicated that $\Delta G^{o}_{ads,NO2\rightarrow TM@C-NG}$ values are almost similar for doped metal transitions of Mn, Co, and Cu on the C-NG nanosheet, while $\Delta G^{o}_{ads,\ CO2\rightarrow TM@C-NG}$ has the largest gap of Gibbs free energy adsorption with dipole moment.

Methods The Langmuir adsorption model with a three-layered ONIOM using CAM-B3LYP functional accompanying LANL2DZ, EPR-III and 6-31 + G (d,p) basis sets due to Gaussian 16 revision C.01 program on the complexes of $CO_2 \rightarrow$ (Fe, Ni, Zn) and $NO_2 \rightarrow$ (Mn, Co, Cu) doped on the C-NG has been accomplished. Then, NMR and IR spectroscopy, nuclear quadrupole resonance, and natural bond orbital analysis have been accomplished for evaluating chemical shielding tensors, thermodynamic properties, electric potential, and occupancy fluctuation through bond orbitals, respectively. In addition, frontier orbitals of LUMO, HOMO, and also a series of chemical reactivity parameters have been calculated. Finally, time-dependent-DFT method due to UV-VIS spectrums has been accomplished to discern the low-lying excited states of CO_2 and NO_2 adsorption on the (Fe, Ni, Zn) and (Mn, Co, Cu), respectively, doped C-NG sheet.

Keywords (Fe, Ni, Zn) @C-NG · (Mn, Co, Cu) @C-NG · Gas sensor · CO_2 · NO_2 · ONIOM/CAM · Langmuir adsorption

Introduction

Sensing and grabbing toxic and harmful gases like CO, CO_2, NO, N_2O, CH_4, SO_2, and H_2S can largely help maintain the human health and the ecosystem [1–3]. Different usages of carbon nanocompounds, such as adsorbing of hydrogen, hazardous compounds, gas, and designing the sensor instruments, have been investigated [4–9].

Nanostructures were applied for various applications consisting of sensing drugs [10], environmental gases [11], and other compounds. Existence of toxic gas in the environment conducts to essential health subjects like swelling throats, delayed nervous system responses, and other health problems.

Recently, the adsorption performances of various metal-doped fullerene surfaces containing $C_{59}Au$, $C_{59}Hf$, $C_{59}Hg$, $C_{59}Ir$, $C_{59}Os$, $C_{59}Pt$, $C_{59}Re$, and $C_{59}W$ on thiourea [$SC(NH_2)_2$] molecule using first-principles density functional theory computation have been done. Louis and coworkers have indicated that $CH_4N_2S@C_{59}Pt$ complex has better sensing characteristics than other compounds in the interactions between thiourea molecule and transition metal-doped fullerene surfaces [12].

Moreover, many materials including carbon structures have been designed and applied as adsorptive removal of

✉ Fatemeh Mollaamin
smollaamin@gmail.com

[1] Department of Biomedical Engineering, Faculty of Engineering and Architecture, Kastamonu University, Kastamonu, Turkey

[2] Department of Chemical Engineering, Central Tehran Branch, Islamic Azad University, Tehran, Iran

environmental pollutant gases [13–15]. Thus, it is essential to make high-implement gas detectors for distinguishing these compounds.

Therefore, remarkable surface of carbon nanostructures is a privileged factor for gas detecting and adsorbing gas devices. In addition, enough implanting of the compounds with transition metals might enhance their adsorbing ability and adjust their adsorbing selectivity as the excellent dopant applicants [16–20].

Because of high emission of greenhouse gases such as CO, CO_2, H_2S, NH_3, NO, NO_2, and SO_2, the study of environmental sustainability has been crucial among the scientists. Recently, the effect of transition metal doped on pristine C_{24} nanocage for increasing gas sensing properties of these structures has been investigated for discovering the adsorption attributes including adsorption energy (E_{ads}), electronic properties, visual study of weak interactions, dipole moment, and recovery time for reusability [21, 22].

Besides, the scientists have approved that nanomaterials of two dimensions (2D) with sizes between 0.1 and 100 nm diameters are employed in the fabrication of nanodevices due to their high surface-to-volume ratio and good compatibility for molecule sensing like hazardous gases [23].

Furthermore, the usage of 3D nano-materials such $Al_{12}N_{12}$, $Ca_{12}O_{12}$, and $Mg_{12}O_{12}$-nanostructured materials as sensors and detectors for several systems have been unraveled by using DFT methods [24].

As a matter of fact, this research wants to investigate the adsorption of hazardous gases of CO_2 and NO_2 on the carbon nanographene which has been decorated by transition metals of iron, nickel, zinc and manganese, cobalt, and copper, respectively, using DFT (density functional theory) approach to discover the adsorbing parameters of the various TM-doped nanographene surface.

Theory, compound and methodology

Toxic gas removal

This study investigates the adsorption of CO_2 and NO_2 onto the transition metal–doped carbon nanographene. This part defines the first process of bond formation arising in the meanwhile of CO_2 and NO_2 chemisorption and runs over the consequents gained for adsorbing of CO_2 and NO_2 onto (Fe, Ni, Zn) and (Mn, Co, Cu), respectively, doping of carbon nanographene. The resulted data from transition metal–doped graphene surface is measured for two toxic gases. Bonding of the CO_2 and NO_2 molecules to a TM atom on the C-NG surface can be observed as first launching by the giving the lone pair on the C-atom into unoccupied d orbitals of the TM atom. The donor potency of CO_2 and NO_2 in this procedure is recognized to be much tiny, and the stability of the TM-C bond is confirmed to be captured by back donation of electrons from occupied d orbitals on the metal into unoccupied antibonding π* orbitals on CO_2 and NO_2 gas molecules.

Study of Langmuir adsorption & charge distribution

Langmuir adsorbing can be illustrated through the physical and chemical interactions on the area of the resembling solid state that adsorb compounds without any interactions with each other making a monolayer of particles on the solid state surface [25, 26].

The Langmuir adsorption is described as follows [27]:

$$\theta_A = \frac{V}{V_m} = \frac{K_{eq}^A p_A}{1 + K_{eq}^A p_A} \quad (1)$$

where θ_A is the fractional occupancy of the adsorbing sites, the ratio of V is the volume of adsorbed gas onto the solid, and V_m is the volume of a monolayer gas particles coating the entire of the solid surface and totally filled by the adsorbate particle. A continuing monolayer of adsorbate particles coating a resembling solid surface is the basic concept for this adsorbing system [28, 29].

Different studies have concentrated on the gas adsorbing susceptibilities of C-nanosurfaces which denote a good accord with the Langmuir adsorbing template. The adsorption of toxic CO_2 and NO_2 gases on the TM-doped graphene nanosheet has been approved by the most appropriate Langmuir isotherm, which indicates the nature of chemisorption for the bond distance between : Ö = C = Ö, : Ö : −Ṅ = Ö : molecules and TM-doped C-nanographene and the equilibrium electron diffusion of the adsorbed particles between the solid and gas phases, and a monolayer feature. The gas molecules of : Ö = C = Öand : Ö : −Ṅ = Ö : are kept on TM-doped C-nanographene with Langmuir chemisorption (Scheme 1).

In fact, the mechanism of the gas sensing phenomenon in (Fe, Ni, Zn) and (Mn, Co, Cu) doping of C-nanographene (adsorbent) would be due to charge transfer between surface and adsorbates of CO_2 and NO_2 molecules, respectively. The changes of charge density analysis in the adsorption process has illustrated that Fe-doped, Ni-doped, and Zn-doped C-nanographene show the atomic charge (coulomb) of −1.345, −2.087, and −1.416, respectively, before adsorption of carbon dioxide, and −1.898, −1.763, and −3.221, respectively, after adsorption of carbon dioxide (Fig. 1a; Table 1). Also, Mn-doped, Co-doped, and Cu-doped C-nanographene have exhibited the atomic charge (coulomb) of −1.499, −2.241, and −1.570, respectively, before adsorption of nitrogen dioxide, and −1.549, −1.794, and −1.708, respectively, after adsorption of nitrogen dioxide (Fig. 1b; Table 2).

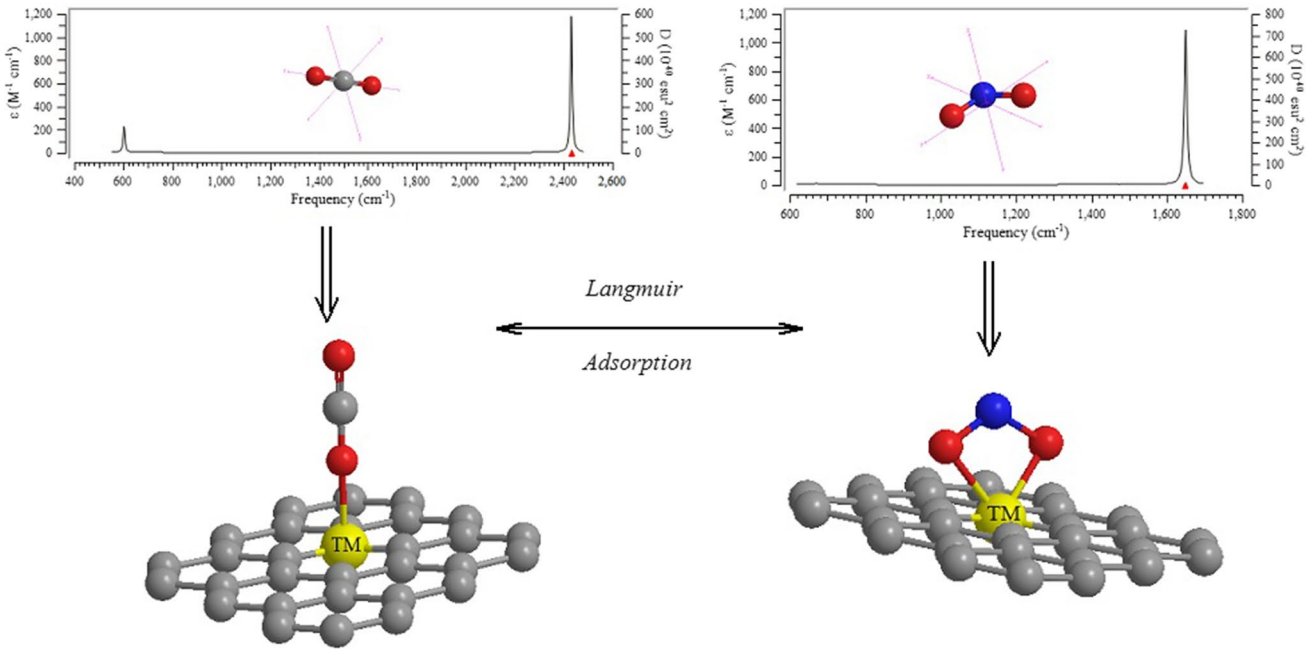

Scheme 1 IR spectrums of :O¨=C=O¨ and :O¨:-N ¨=O¨: molecules which adsorb on (Fe, Ni, Zn) and (Mn, Co, Cu), respectively, doping of C-nanographene.

Therefore, the changes of charge density for Langmuir adsorption of carbon dioxide on Fe-doped, Ni-doped, and Zn-doped C-nanographene alternatively are $\Delta Q_{\text{Ni-doped}} = +0.324 \lll \Delta Q_{\text{Fe-doped}} = -0.553 \ll \Delta Q_{\text{Zn-doped}} = -1.805$ (Fig. 1a; Table 1). The values of changes of charge density have illustrated a more significant charge transfer for Ni-doped C-nanographene. Furthermore, the changes of charge density for Langmuir adsorption of nitrogen dioxide on Mn-doped, Co-doped, and Cu-doped C-nanographene alternatively are $\Delta Q_{\text{Co-doped}} = +0.447 \lll \Delta Q_{\text{Mn-doped}} = -0.05 \ll \Delta Q_{\text{Cu-doped}} = -0.138$. The values of changes of charge density have denoted a more significant charge transfer for Co-doped C-nanographene (Fig. 1b; Table 2).

The methodology of ONIOM

N-layered integrated molecular orbital and molecular mechanics or ONIOM merges three theoretical levels for reducing the sequence of validity as the high, medium, and low degrees of theory. In this model, high-degree level has been performed using the density functional theory insight of CAM-B3LYP wave function with 6-31 + G (d, p) basis set for some carbon atoms in nanographene and oxygen atoms in the adsorption zone and EPR-III basis set for nitrogen and LANL2DZ for some iron, nickel, zinc and manganese, cobalt, and copper atoms through adsorbing CO_2 and NO_2, respectively, in the adsorption zone. Medium-degree level has been considered on the other carbon atoms of nanographene in the adsorption zone owing to semi-empirical methodologies. At last, a low-degree level has been depicted on the other iron, nickel, zinc and manganese, cobalt, and copper atoms, through adsorption of CO_2 and NO_2, respectively, with MM2 force fields of molecular mechanic methods, $E_{\text{ONIOM}} = E_{\text{High}} + E_{\text{Medium}} + E_{\text{Low}}$ (Scheme 2) [30].

In other words, the three-degree model of ONIOM leads to explore a ground order more precisely than the one-degree model which might treat a medium size order exactly such as a huge order with admissible validity [31].

In this article, the structures have been computed by using CAM-DFT method on the mechanisms of adsorption of CO_2 and NO_2 by (Fe, Ni, Zn) and (Mn, Co, Cu), respectively, doping of C-nanographene through bonding between transition metals and gas molecule. It has been discovered that the surface binding zone preference of O-atom of CO_2 and N-atom of NO_2, respectively, in adsorption zone is greatly influenced by the existence of neighboring atoms in the C-nanographene. The calculated of pair distribution functions in $CO_2 \rightarrow$ Fe/Ni/Zn and $NO_2 \rightarrow$ Mn/Co/Cu doping of C-NG have depicted that the creation of complexes lead to shorter bond lengths of O → Fe, O → Ni, and O → Zn and N → Mn, N → Co, and N→ Cu, respectively, once balanced to the analogous increment (Scheme 2).

Concerning DFT or density functional theory, hybrid functional is considered a series of approximations for the exchange-correlation energy functional which merges a sector of precise exchange from HF or Hartree-Fock theory methodology with the remainder of the exchange-correlation energy from other notifications like empirical

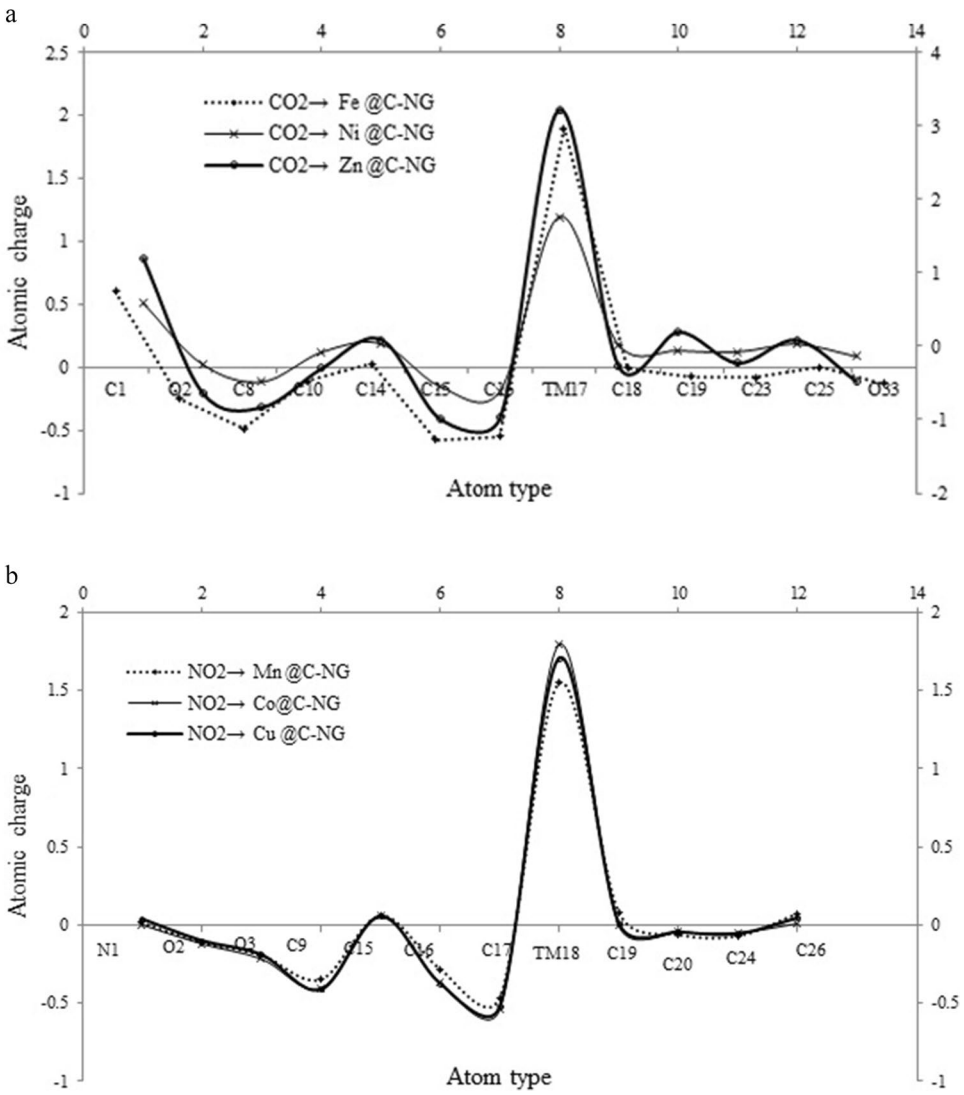

Fig. 1 The changes of charge density analysis in the adsorption process showing that Fe-doped, Ni-doped, and Zn-doped C-nanographene and Mn-doped, Co-doped, and Cu-doped C-nanographene have exhibited atomic charge

or ab initio approaches. Thus, the precise exchange energy functional is represented by the Kohn-Sham orbitals in lieu of density, therefore, is located as the indirect density functional. This research has employed the impression of the hybrid functional of three-parameter basis set of Becke, Lee, Yang, Parr (B3LYP) within the skeleton of DFT upon theoretical computations [32, 33].

Moreover, the dispersion corrected DFT-D3 energy $E_{\mathrm{DFT-D}}$ is calculated by adding the empirical correction energy E_{disp} to the DFT energy E_{DFT} as formula [34, 35]:

$$\Delta E_{\mathrm{DFT-D3}} = \Delta E_{\mathrm{DFT}} - \Delta E_{\mathrm{disp}} \tag{2}$$

Therefore, from third-order perturbation theory, one gets the Axilrod–Teller–Muto dispersion term for the consideration of the non-additivity of dispersion interaction:

$$\mathrm{D3(ABC)} = \sum_{ABC} f_{\mathrm{damp}} \frac{C_9^{ABC}\left(3\cos\left(\theta_a\right)\ \cos\left(\theta_b\right)\cos\left(\theta_c\right)+1\right)}{r_{AB}r_{BC}r_{CA}} \tag{3}$$

where C_9^{ABC} coefficients are the geometric mean of the C_6-coefficients; θ_a, θ_b, and θ_c are the angles of the triangle, which is formed by the three atoms; and f_{damp} is the damping function. The Axilrod–Teller–Muto dispersion terms can be ignored for molecular systems [34].

In this work, it has been also carried out the calculations with the PBE-D3 approach using cutoff energy for the plane-wave valence basis and a $3 \times 3 \times 1$ k-point mesh for reciprocal-space integration. A preliminary convergence investigation has exhibited that these amounts are an optimal compromise between accuracy and computational yield.

Transition metal–doped graphene sheet has been made by hard system and Z-matrix format of which a blank line has been positioned. The hard potential energy surface has been exposed at CAM-B3LYP functional [36], and concerning LANL2DZ/6-31 + G (d,p) basis sets to appoint frontier molecular orbital, atomic charges, nuclear magnetic resonance properties, dipole

Table 1 The changes of charge density analysis in the adsorption process

$CO_2 \rightarrow$ Fe @C-NG				$CO_2 \rightarrow$ Ni@ C-NG				$CO_2 \rightarrow$ Zn@C-NG			
Atom	σ_{iso}	σ_{aniso}	Q	Atom	σ_{iso}	σ_{aniso}	Q	Atom	σ_{iso}	σ_{aniso}	Q
C1	148.52	196.31	0.5999	C1	178.24	145.52	0.5848	C1	123.10	234.73	1.1957
O2	321.65	183.04	−0.2528	O2	398.64	64.18	−0.2501	O2	295.29	190.97	−0.6366
C8	100.76	347.30	−0.4878	C8	296.58	574.94	−0.4852	C8	273.90	3225.40	−0.8329
C10	237.59	173.64	−0.1115	C10	41.45	461.74	−0.0808	C10	292.83	1382.14	−0.3038
C14	240.60	485.27	0.0250	C14	68.33	371.25	0.0338	C14	463.91	927.12	0.0904
C15	237.40	341.12	−0.5742	C15	94.84	252.27	−0.5501	C15	534.07	1981.05	−0.9951
C16	183.26	383.67	−0.5461	C16	25.48	160.68	−0.6144	C16	1163.51	3304.01	−0.9772
Fe 17	21,368.96	19,790.99	1.8981	Ni17	7265.00	43,068.15	1.7629	Zn 17	1374.46	528.33	3.2211
C18	40.19	130.77	−0.0049	C18	304.39	798.78	0.0153	C18	233.95	593.95	−0.2791
C19	739.86	1981.10	−0.0750	C19	1620.91	4749.68	−0.0591	C19	5571.71	12698.28	0.1942
C23	93.25	179.03	−0.0816	C23	68.71	216.09	−0.0767	C23	127.04	228.84	−0.2287
C25	267.56	385.81	0.0005	C25	130.48	138.07	0.0295	C25	630.19	1178.08	0.0828
O33	284.15	153.28	−0.1321	O33	343.76	111.69	−0.1407	O33	293.15	160.22	−0.4784

The chemical shielding (CS) tensors in principal axis system evaluate the isotropic chemical-shielding (σ_{iso}), anisotropic chemical-shielding (σ_{aniso}) [39]: $\sigma_{iso} = \frac{\sigma 33+\sigma 22+\sigma 11}{3}$; $\sigma_{aniso} = \sigma 33 - \frac{\sigma 22+\sigma 11}{2}$

Table 2 The values of changes of charge density of Mn-doped, Co-doped, and Cu-doped C-nanographene

: Ö : −Ṅ = Ö :→ Mn@ C-NG			: Ö : −Ṅ = Ö :→ Co@ C-NG			: Ö : −Ṅ = Ö :→ Cu @C-NG		
Atom type	E_p	Q	Atom type	E_p	Q	Atom type	E_p	Q
N1	−17.8974	0.0138	N1	−17.9023	0.0001	N1	−17.8793	0.0395
O2	−21.7065	−0.1115	O2	−21.7065	−0.1212	O2	−21.6890	−0.0991
O3	−21.9267	−0.1936	O3	−21.9372	−0.2173	O3	−21.9183	−0.1888
C9	−14.5480	−0.3492	C9	−14.5398	−0.4064	C9	−14.5414	−0.4128
C15	−14.4653	0.0591	C15	−14.4733	0.0599	C15	−14.4885	0.0551
C16	−14.4560	−0.2814	C16	−14.4737	−0.3711	C16	−14.4885	−0.3726
C17	−14.5684	−0.4658	C17	−14.6058	−0.5429	C17	−14.6196	−0.5217
Mn 18	−107.7744	1.5486	Co 18	−120.312	1.7938	Cu 18	−133.3453	1.7077
C19	−14.4372	0.0776	C19	−14.5038	−0.0058	C19	−14.4900	0.0091
C20	−14.6675	−0.0628	C20	−14.6703	−0.0463	C20	−14.6639	−0.0430
C24	−14.4956	−0.0711	C24	−14.5033	−0.0499	C24	−14.5126	−0.0561
C26	−14.4425	0.0725	C26	−14.4941	0.0094	C26	−14.5053	0.0468

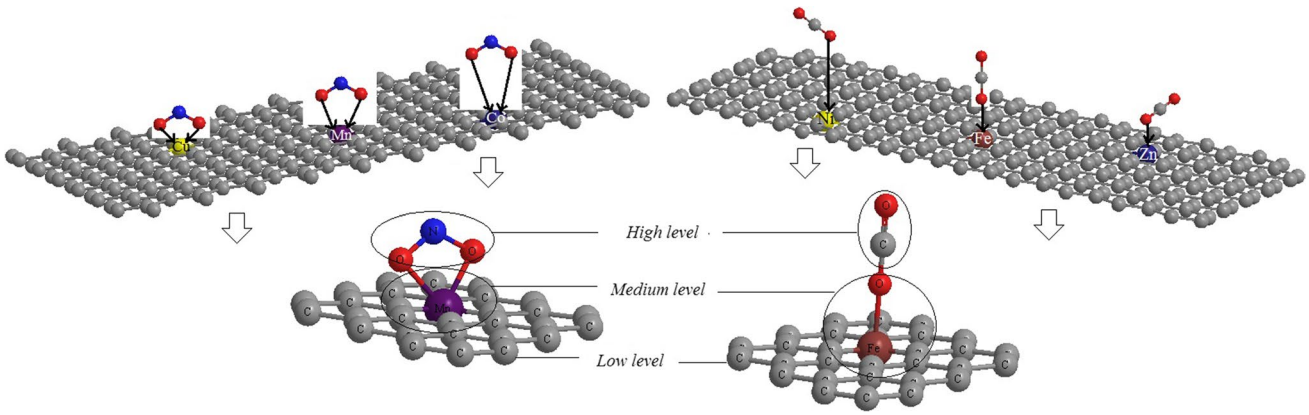

Scheme 2 Langmuir adsorbing of CO2 and NO2 as the toxic gas pollutant onto (Fe, Ni, Zn) and (Mn, Co, Cu), respectively, doping of C-nanographene graphene on optimized structure due to three-degree layered of high, medium and low levels of ONIOM model.

moment, thermodynamic characteristics, and other quantum attributes [37]. In this research, CO_2 and NO_2 have been adsorbed onto TM-doped C-nanographene toward formation of CO_2 → Fe/Ni/Zn and NO_2 → Mn/Co/Cu, respectively, doping of C-NG sheet using Gaussian 16 revision C.01 program [38].

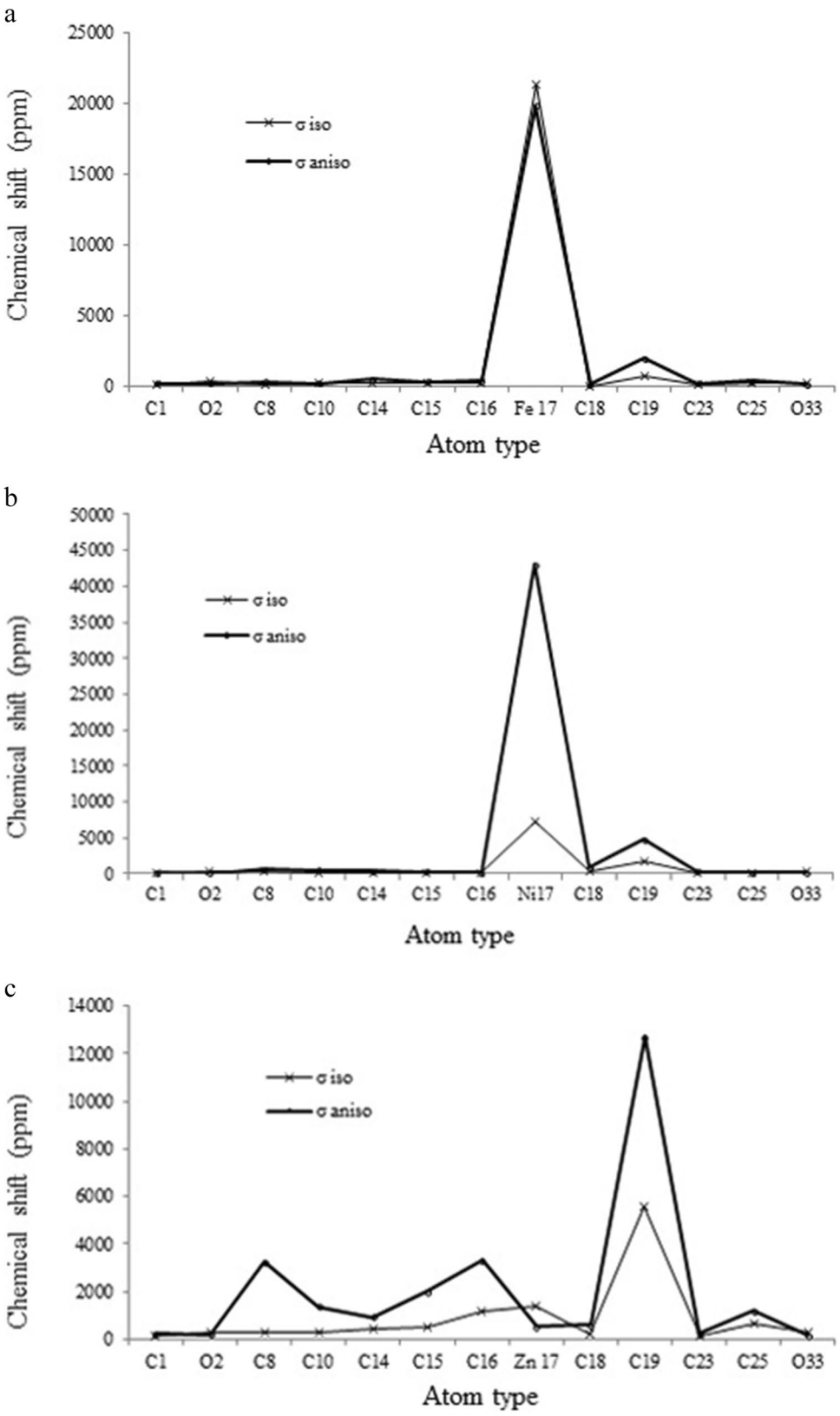

Fig. 2 The chemical shielding (ppm) behavior for CO_2 adsorption on the (Fe, Ni, Zn)-doped carbon nanographene

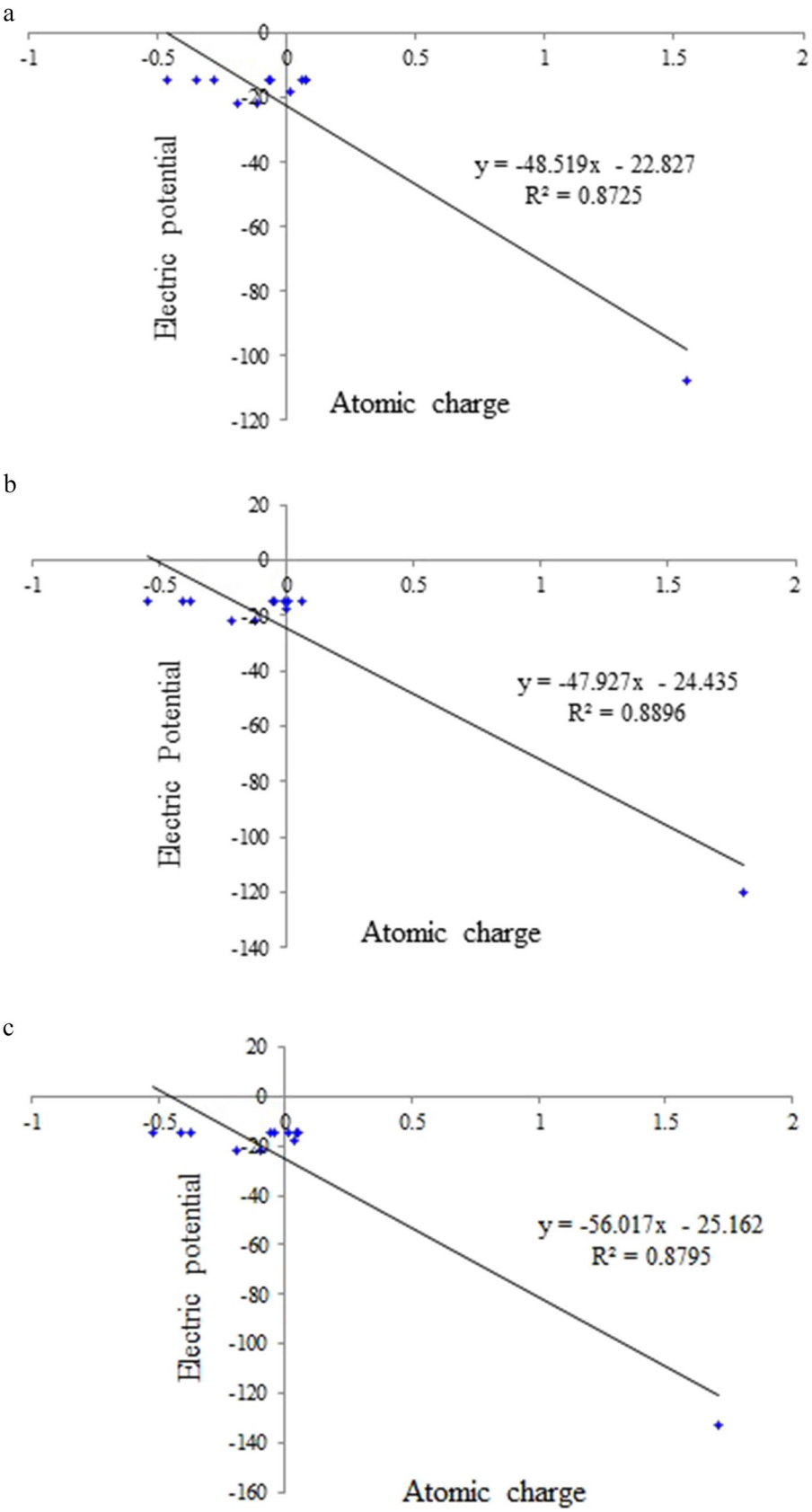

Fig. 3 The electric potential of NQR method versus atomic charge for elements of : Ö : −Ṅ = Ö : → (Mn, Co, Cu)-doped nanographene

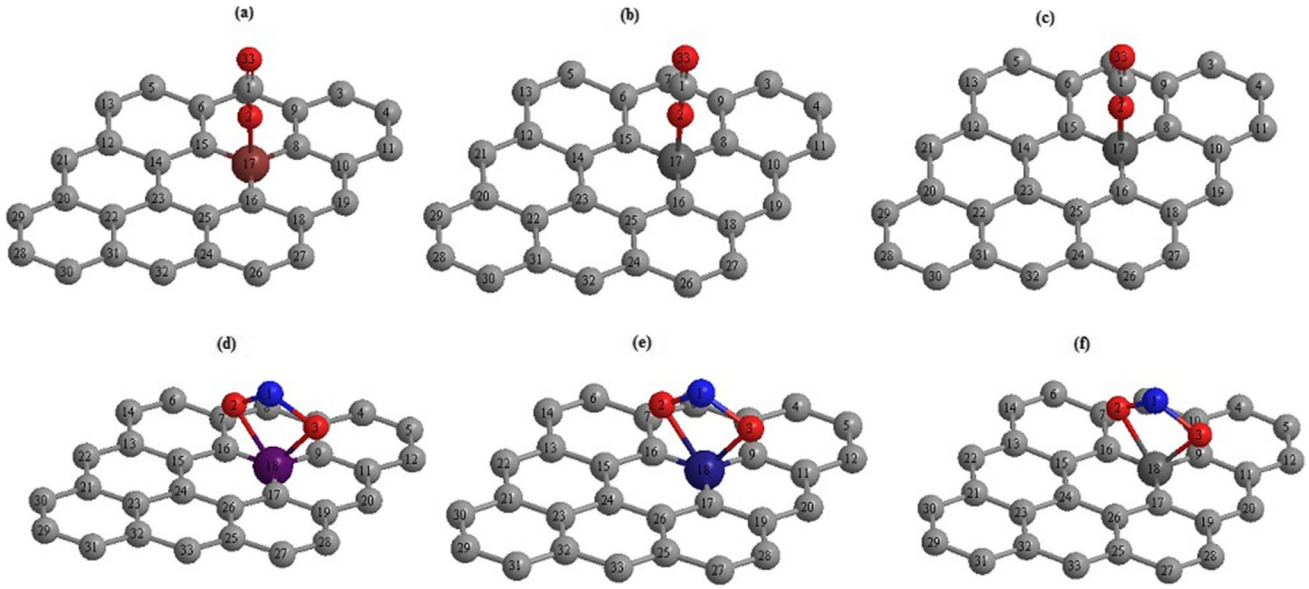

Scheme 3 Optimized structures of CO2 adsorbed on the (Fe, Ni, Zn) -doped C-NG and NO2 adsorption on the (Mn, Co, Cu) -doped C-NG.

Results and discussion

In this investigation, transition metals of manganese, iron, cobalt, nickel, copper and zinc doped on the nanographene have been investigated as the efficient surfaces for adsorption toxic gases of carbon dioxide (CO_2) and nitrogen dioxide (NO_2) causing air pollution. These experiments have been accomplished using spectroscopy analysis through some physico-chemical attributes.

NMR spectroscopy

Concerning nuclear magnetic resonance spectroscopy, parameters of isotropic (σ_{iso}), and anisotropy (σ_{aniso}) shielding tensors of NMR spectroscopy for certain atoms in the active site of CO_2 adsorption on the (Fe, Ni, Zn)-doped carbon nanographene through the creation of the binding between gas molecules and solid surface have been evaluated by using Gaussian 16 revision C.01 program and represented in Table 1 [38, 39].

Considering Fig. 2a–c, it has been depicted the degeneracy of NMR graphs via chemical shielding (ppm) for CO_2 adsorption on the (Fe, Ni, Zn)-doped carbon nanographene.

The graphs of NMR spectroscopy in Fig. 2a, b have shown approximately the identical chemical shielding behavior of isotropic and anisotropy parameters for $CO_2 \rightarrow$ Fe @C-NG, and $CO_2 \rightarrow$ Ni @C-NG with a the sharp peaks close to Fe(17) and Ni(17) doping on the surface of nanographene, respectively. However, it has been observed several fluctuations around the graph of Zn-doped on the nanographene surface and a sharp peak near C(19) in the neighbor of junction between atom type O(2) from carbon dioxide (CO_2) and Zn (17) form Zn-doped on the nanographene (Fig. 2c). However, NO_2 adsorption on the Mn-, Co-, and Cu-doped graphene surface compared to CO_2 adsorption on the Fe-, Ni-, and Zn-doped graphene surface could not exhibit the acceptable chemical shielding behavior of isotropic and anisotropy parameters.

Study of NQR

Nuclear quadrupole resonance (NQR) method has been carried out for the complexes of NO_2 adsorption on the (Mn, Co, Cu)-doped carbon nanographene. NQR is based on the multipole enlargement in Cartesian harmonies as the following equations:

$$V(r) = V(0) + \left[\left(\frac{\partial V}{\partial x_i}\right)|_0 .x_i\right] + \frac{1}{2}\left[\left(\frac{\partial^2 V}{\partial x_i x_j}\right)|_0 .x_i x_j\right] + \ldots \tag{4}$$

Then, after simplification the equation, there are only the second derivatives dependent on the same variable for the potential energy [40, 41]:

$$\begin{aligned} U &= -\frac{1}{2}\int_{\mathcal{D}} d^3 r \rho_r \left[\left(\frac{\partial^2 V}{\partial x_i^2}\right)|_0 .x_i^2\right] \\ &= -\frac{1}{2}\int_{\mathcal{D}} d^3 r \rho_r \left[\left(\frac{\partial E_i}{\partial x_i}\right)|_0 .x_i^2\right] \\ &= -\frac{1}{2}\left(\frac{\partial E_i}{\partial x_i}\right)\Big|_0 \cdot \int_{\mathcal{D}} d^3\, r\, \left[\rho(r).x_i^2\right] \end{aligned} \tag{5}$$

Table 3 The natural bond orbital (NBO) analysis of CO_2 adsorbed on the (Fe, Ni, Zn)-doped carbon nanographene and NO_2 adsorption

Gas molecules → TM-doped carbon nanographene	Bond orbital	Occupancy	Hybrids
: Ö = C = Ö :→ Fe @C-NG	BD (1) C1–O2	1.9895	0.6388 ($sp^{1.03}$) C + 0.7694 ($sp^{3.01}$) O
	BD (1) C1–O3	1.9975	0.6503 ($sp^{0.97}$) C + 0.7597 ($sp^{2.93}$) O
	BD (1) C8–Fe17	1.9573	0.8077 ($sp^{1.70}$) C + 0.5895 ($sp^{0.31}$ $d^{3.23}$) Fe
	BD (1) C15–Fe17	1.9528	0.8178 ($sp^{1.40}$) C + 0.5756 ($sp^{0.36}$ $d^{3.29}$) Fe
	BD (1) C16–Fe17	1.9613	0.8196 ($sp^{1.46}$) C + 0.5730 ($sp^{0.4}$ $d^{4.24}$) Fe
: Ö = C = Ö :→ Ni @C-NG	BD (1) C1–O2	1.9894	0.6430 ($sp^{1.02}$) C + 0.7659 ($sp^{3.25}$) O
	BD (1) C1–O3	1.9974	0.6498 ($sp^{0.98}$) C + 0.7601 ($sp^{2.91}$) O
	BD (1) C8–Ni17	1.9682	0.8015 ($sp^{1.58}$) C + 0.5980 ($sp^{0.34}$ $d^{1.91}$) Ni
	BD (1) C15–Ni17	1.9682	0.8098 ($sp^{1.38}$) C + 0.5868 ($sp^{0.38}$ $d^{2.13}$) Ni
	BD (1) C16–Ni17	1.9745	0.8219 ($sp^{1.44}$) C + 0.5697 ($sp^{0.67}$ $d^{4.65}$) Ni
: Ö = C = Ö :→ Zn @C-NG	BD (1) C1–O2	1.9948	0.5712 ($sp^{0.99}$) C + 0.8208 ($sp^{1.51}$) O
	BD (1) C1–O3	1.9979	0.5802 ($sp^{1.02}$) C + 0.8145 ($sp^{1.50}$) O
	BD (1) C8–Zn17	1.9643	0.6481 ($sp^{1.39}$) C + 0.7616 ($sp^{0.37}$ $d^{2.47}$) Zn
	BD (1) C15–Zn17	1.9592	0.7035 ($sp^{1.19}$) C + 0.7107 ($sp^{0.33}$ $d^{3.15}$) Zn
	BD (1) C16–Zn17	1.9287	0.7038 ($sp^{1.25}$) C + 0.7104 ($sp^{0.62}$ $d^{4.67}$) Zn
: Ö : −Ṅ = Ö :→ Mn @C-NG	BD (1) N1–O2	1.9482	0.6446 ($sp^{3.94}$) N + 0.7645 ($sp^{4.00}$) O
	BD (1) N1–O3	1.9311	0.7591 ($sp^{3.20}$) N + 0.6509 ($sp^{4.15}$) O
	BD (1) C9–Mn18	1.9329	0.7563 ($sp^{1.75}$) C + 0.6543 ($sp^{0.20}$ $d^{4.96}$) Mn
	BD (1) C16–Mn18	1.9103	0.8161 ($sp^{1.69}$) C + 0.5779 ($sp^{0.80}$ $d^{2.09}$) Mn
	BD (1) C17–Mn18	1.9496	0.7660 ($sp^{1.55}$) C + 0.6428 ($sp^{0.33}$ $d^{4.15}$) Mn
: Ö : −Ṅ = Ö :→ Co @C-NG	BD (1) N1–O2	1.9443	0.6399 ($sp^{3.97}$) N + 0.7684 ($sp^{3.54}$) O
	BD (1) N1–O3	1.9248	0.7538 ($sp^{3.17}$) N + 0.6571 ($sp^{3.69}$) O
	BD (1) C9–Co18	1.9641	0.8409 ($sp^{1.29}$) C + 0.5412 ($sp^{0.88}$ $d^{2.85}$) Co
	BD (1) C16–Co18	1.9557	0.8444 ($sp^{1.50}$) C + 0.5358 ($sp^{1.14}$ $d^{2.04}$) Co
	BD (1) C17–Co18	1.9734	0.8330 ($sp^{1.30}$) C + 0.5533 ($sp^{0.79}$ $d^{4.09}$) Co
: Ö : −Ṅ = Ö :→ Cu @C-NG	BD (1) N1–O2	1.9460	0.6398 ($sp^{3.96}$) N + 0.6398 ($sp^{3.45}$) O
	BD (1) N1O3	1.9220	0.7579 ($sp^{3.16}$) N + .6524 ($sp^{3.60}$) O
	BD (1) C9–Cu18	1.9044	0.8390 ($sp^{1.21}$) C + 0.5442 ($sp^{2.33}$ $d^{1.63}$) Cu
	BD (1) C16–Cu18	1.9658	0.8422 ($sp^{1.43}$) C + 0.5392 ($sp^{0.94}$ $d^{1.52}$) Cu
	BD (1) C17–Cu18	1.9494	0.8390 ($sp^{0.98}$) C + 0.5442 ($sp^{1.81}d^{1.30}$) Cu

There are two parameters which must be gotten from NQR experiments: the quadrupole coupling constant, χ, and asymmetry parameter of the EFG tensor η:

$$\chi = {e^2 Q q_{zz}}/{h} \tag{6}$$

$$\eta = {q_{xx} - q_{yy}}/{q_{zz}} \tag{7}$$

where q_{ii} are components of the EFG tensor at the quadrupole nucleus determined in the EFG principal axes system, Q is the nuclear quadrupole moment, e is the proton charge, and h is the Planck's constant [42].

The electric potential ($J{\cdot}C^{-1}$) is a continuous function in space produced by an idealized point charge has $1/r$ potential:$V_E = \frac{1}{4\pi\varepsilon_0}\frac{Q}{r}$, where Q (measured in coulombs) is the point charge, r is the distance from the charge, and ε_0 is the permittivity of vacuum.

Since the electric potential for a system of point charges is equal to the sum of the point charges' individual potentials, the calculations are done simply based on summation of potential fields which is scalar instead of summation of the electric fields that is vector and much more difficult that potential field. So, $V_E(r) = \frac{1}{4\pi\varepsilon_0}\sum_i \frac{q_i}{|r-r_i|}$, where r is a point at which the potential is measured, r_i is a point at which the charge is ≠0, and q_i is the charge at the point r_i. Finally, the potential of a continuous charge distribution $\rho(r)$ appears:$V_E(r) = \frac{1}{4\pi\varepsilon_0}\int_R \frac{\rho(r')}{|r-r'|}\,d^3r'$, where R is a region including

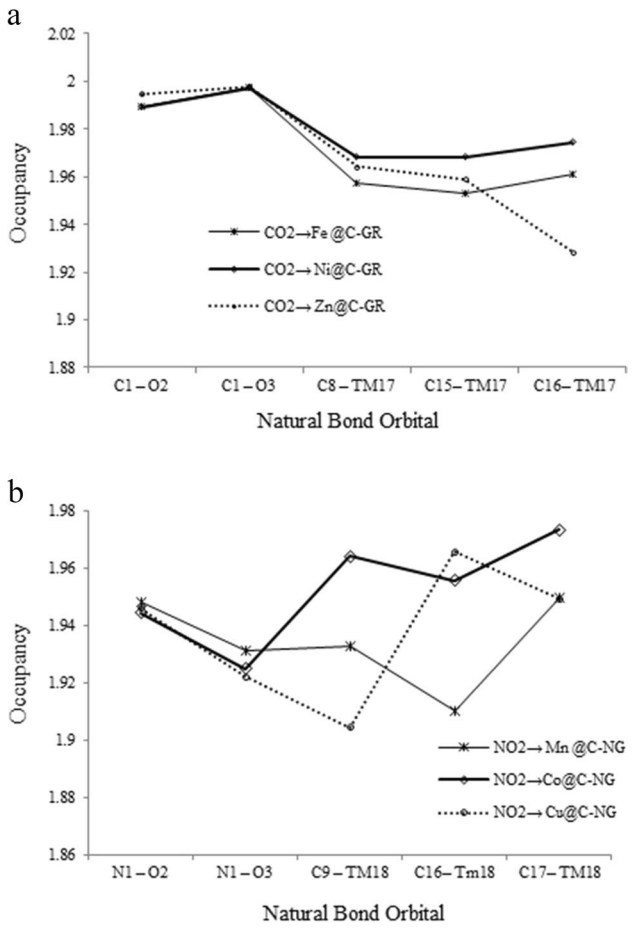

Fig. 4 The character of electronic conjugation between bonds in the gas molecules and TM@C-NG

all the points at which the charge density is ≠0, r' is a point inside R, and $\rho(r')$ is the charge density at the point r' [43].

As the EFG at the position of the nucleus in gas adsorbed on the metal-doped carbon nanographene as the gas sensor is assigned by the valence electrons twisted in the special linkage with close nuclei of C-nanographene surface, the NQR frequency at which transitions happen is particular for: Ö : $-\dot{N}=$ Ö :→ (Mn, Co, Cu)-doped C-nanographene (Table 2).

In addition, in Fig. 3a–c, it has been plotted the electric potential of NQR method versus atomic charge for elements of : Ö : $-\dot{N}=$ Ö :→ (Mn, Co, Cu)-doped nanographene using CAM-B3LYP/EPR-III, LANL2DZ, 6-31 + G (d,p) level of theory.

In Fig. 3a–c, it has been remarked the changes of electric potential for nitrogen, oxygen, carbon, manganese, cobalt, and copper in the active site of Langmuir adsorption. In fact, it has been observed the effect of the substitution of carbon atoms in pristine graphene with manganese, cobalt, and copper, during adsorbing NO_2 through resulted electric potential using NQR analysis (Fig. 3a–c). It is obvious that the graphs of : Ö : $-\dot{N}=$ Ö :→ Mn@C-NG with $R^2 = 0.8725$ (Fig. 3a): Ö : $-\dot{N}=$ Ö :→ Co@C-NG with $R^2 = 0.8896$ (Fig. 3b), and: Ö : $-\dot{N}=$ Ö :→ Cu@C-NG with $R^2 = 0.8795$ (Fig. 3c), are fluctuated by Mn, Co, and Cu, respectively, which represent the efficiency of nitrogen dioxide detectors as the promising scavengers. However, CO_2 adsorption on the Fe-, Ni-, and Zn-doped graphene surface compared to NO_2 adsorption on the Mn-, Co-, and Cu-doped graphene surface could not indicate the acceptable values through relation coefficient graphs of electric potential versus atomic charge graphs in the adsorption site of transitions metal doped graphene surface.

Analysis of NBO

Furthermore, the natural bond orbital (NBO) analysis of CO_2 adsorbed on the (Fe, Ni, Zn)-doped carbon nanographene and NO_2 adsorption on the (Mn, Co, Cu)-doped carbon nanographene (Scheme 3) has illustrated the character of electronic conjugation between bonds in the gas molecules and TM@C-NG (Table 3; Fig. 4).

In Fig. 4a, it has been observed the fluctuation of occupancy of natural bond orbitals for CO_2 → Fe@C-NG, CO_2 → Ni@C-NG, and CO_2 → Zn@C-NG surfaces through the Langmuir adsorption process by indicating the active oxygen atom in carbon dioxide becoming close to the nanographene. Moreover, in Fig. 4b, the complexes of NO_2 → Mn@ C-NG, NO_2 → Co@ C-NG, and NO_2 → Cu@ C-NG surfaces have exhibited the most fluctuated graphs through the occupancy via the natural bond orbitals due to the Langmuir adsorption while the active oxygen atoms in nitrogen dioxide becoming close to the C-nanographene (Scheme 3).

The values of changes of charge density have shown a more important charge transfer from nitrogen of : Ö : $-\dot{N}=$ Ö : molecule and oxygen of : Ö = C = Ö : as the electron donors adsorbed onto transition metal doped graphene surfaces which act as the electron acceptors (N → TM@ C-NG, O → TM@ C-NG). In fact, the sites of Fe-, Ni-, Zn-doped carbon graphene and Mn-, Co-, Cu-doped carbon graphene surfaces have higher interaction energy from Van der Waals' forces with NO_2 and CO_2 molecules that can make them highly stable toward adsorption information on the surface. It has been assumed that the priority for selecting the surface binding of N-atom in NO_2 and O-atom in CO_2 in adsorption metal transition sites can be impacted by the existence of close atoms of carbon in graphene surface through co-adsorption phenomenon (Scheme 3) [44, 45].

Thermodynamic properties and IR spectroscopy analysis

Thermodynamic parameters have been estimated for adsorption of toxic carbon dioxide (: Ö = C = Ö :) and nitrogen dioxide (: Ö : $-\dot{N}=$ Ö :) on the surfaces of (Fe, Ni, Zn) and

Table 4 Adsorption of toxic carbon dioxide and nitrogen dioxide

Compound	$\Delta E^{\circ} \times 10^{-4}$ (kcal/mol)	$\Delta E^{\circ}_{\text{DFT-D3}} \times 10^{-4}$	$\Delta H^{\circ} \times 10^{-4}$ (kcal/mol)	$\Delta G^{\circ} \times 10^{-4}$ (kcal/mol)	$\Delta G^{\circ}_{\text{ads}} \times 10^{-4}$ (kcal/mol)	S° (Cal/K mol)	Dipole moment (Debye)
: Ö = C = Ö :	−11.6121	-	−11.6121	−11.6136	-	51.378	0.0000
: Ö : −Ṅ = Ö :	−12.6298	-	−12.6298	−12.6315	-	57.792	0.2323
Fe@ C-NG	−146.2783	-	−146.2782	−146.2816	-	111.175	2.3199
Ni@ C-NG	−162.4794	-	−162.4793	−162.4828	-	116.150	13.6226
Zn@ C-NG	−178.2031	-	−178.2030	−178.2066	-	120.533	1.7301
Mn@ C-NG	−139.3551	-	−139.3551	−139.3588	-	124.779	1.4652
Co@ C-NG	−153.7094	-	−153.7094	−153.7133	-	128.964	0.9321
Cu@ C-NG	−169.6604	-	−169.6605	−169.6643	-	129.753	1.0422
: Ö = C = Ö :→ Fe @C-NG	−157.8893	−157.9004	−157.8893	−157.8932	0.002	130.634	14.1988
: Ö = C = Ö :→ Ni @C-NG	−173.0324	−173.0433	−173.0323	−173.0360	1.0604	122.276	12.5830
: Ö = C = Ö :→ Zn @C-NG	−191.0952	−191.1059	−191.0951	−191.0989	−1.2787	127.012	2.0963
: Ö : −Ṅ = Ö :→ Mn @C-NG	−151.9008	−151.9114	−151.9008	−151.9045	0.0858	125.163	10.5640
: Ö : −Ṅ = Ö :→ Co @C-NG	−166.2564	−166.2671	−166.2564	−166.2598	0.0850	116.087	4.6108
: Ö : −Ṅ = Ö :→ Cu @C-NG	−182.2074	−182.2183	−182.2073	−182.2110	0.0848	123.268	4.1641

(Mn, Co, Cu), respectively, doping of nanographene as the gas sensors which can be used as the selective detectors for environmental hazardous gases (Table 4).

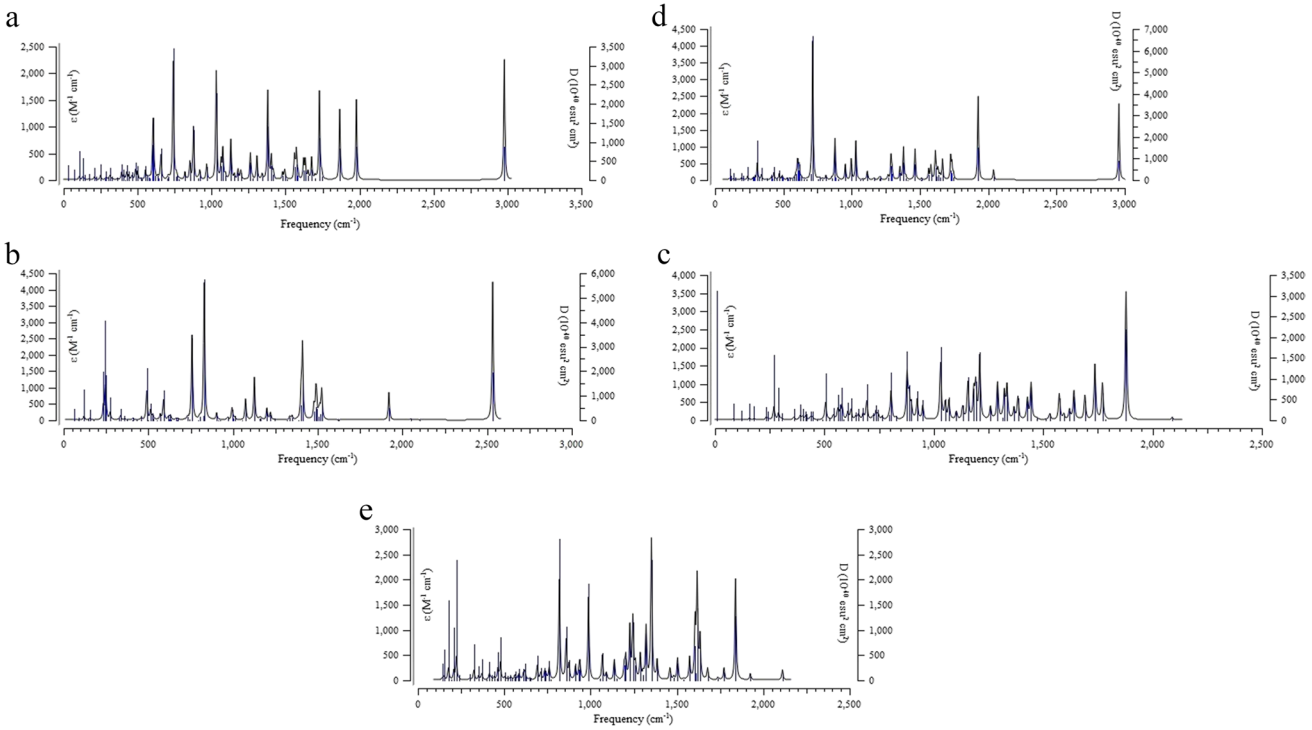

Fig. 5 The graphs of : Ö = C = Ö :→ Fe @C-NG, : Ö = C = Ö :→ Ni @C-NG, and : Ö = C = Ö :→ Zn @C-NG with frequency range around 500–3000 cm^{-1}

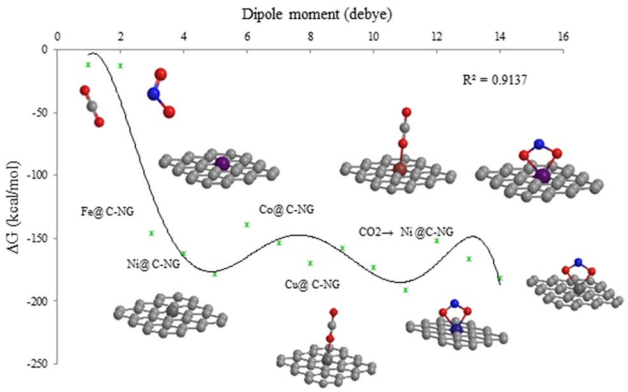

Fig. 6 The maximum of the Langmuir adsorbing isotherm plots related to ΔG^{o}_{ads} versus dipole moment

Furthermore, the infrared spectrums for adsorption of CO_2 by (Fe, Ni, Zn)-doped and NO_2 by (Mn, Co, Cu)-doped, respectively, onto C-nanographene have been reported in Fig. 5a–f.

The graphs of $:\ddot{O}=C=\ddot{O}:\rightarrow$ Fe @C-NG, $:\ddot{O}=C=\ddot{O}:\rightarrow$ Ni @C-NG, and $:\ddot{O}=C=\ddot{O}:\rightarrow$ Zn @C-NG have shown the frequency range around 500–3000 cm^{-1} with the strongest peaks in IR spectrum around 750 cm^{-1} and 3000 cm^{-1} (Fig. 5a–c). In addition, the graphs have been observed in the frequency limitation about 500–2000 cm^{-1} for the complexes of: $:\ddot{O}:-\dot{N}=\ddot{O}:\rightarrow$ Mn @C-NG, $:\ddot{O}:-\dot{N}=\ddot{O}:\rightarrow$ Co @ C-NG, and $:\ddot{O}:-\dot{N}=\ddot{O}:\rightarrow$ Cu @C-NG with the strongest peaks in IR spectrum around 1550 cm^{-1} and 1900 cm^{-1} (Fig. 5d–f).

From Fig. 6, it could be understood that the maximum of the Langmuir adsorbing isotherm plots related to ΔG^{o}_{ads} versus dipole moment may depend on the interactions between the CO_2, NO_2 and TM-doped C-nanographene. The order of Gibbs free energy changes for clusters of gas (donor) → TM@ C-NG (acceptor) is $\Delta G^{0}_{CO2\rightarrow Zn@C} > \Delta G^{0}_{CO2\rightarrow\ Ni@C} > \Delta G^{0}_{CO2\rightarrow Fe@C}$ and $\Delta G^{0}_{NO2\rightarrow Mn@C} > \Delta G^{0}_{NO2\rightarrow Co@C} > \Delta G^{0}_{NO2\rightarrow Cu@C}$, respectively (Table 4; Fig. 6).

The adsorptive capacity of CO_2 and NO_2 on the TM-doped C-nanographene is approved by the ΔG^{o}_{ads} amount:

$$\Delta G^{o}_{ads,CO2} = \Delta G^{o}_{CO2\rightarrow TM@C-NG} - \left(\Delta G^{o}_{CO2} + \Delta G^{o}_{TM@C-NG}\right);(TM = Fe, Ni, Zn) \quad (8)$$

$$\Delta G^{o}_{ads,NO2} = \Delta G^{o}_{NO2\rightarrow TM@C-NG} - \left(\Delta G^{o}_{NO2} + \Delta G^{o}_{TM@C-NG}\right);(TM = Mn, Co, Cu) \quad (9)$$

On the basis of data in Table 4, it is predicted that the adsorption of CO_2 and NO_2 on the TM-doped graphene nanosheet must be physico-chemical attributes. As seen in Fig. 6, all the calculated $\Delta G^{o}_{ads,NO2}$ values are approximately identical similar for three metal transitions of Mn, Co, and Cu, but $\Delta G^{o}_{ads,\ CO2}$ (-1.2787×10^{-4}, kcal/mol) has the largest gap of Gibbs free energy adsorption with dipole moment which defines the alterations between Gibbs free energy of initial compounds (ΔG^{o}_{CO2} and $\Delta G^{o}_{Zn@C-NG}$) and product compound ($\Delta G^{o}_{CO2\rightarrow Zn@C-NG}$) through polarizability. In fact, TM-doped C-nanographene can possess enough efficiency for adsorption toxic gases of carbon dioxide and nitrogen dioxide through charge transfer from nitrogen and oxygen atoms, respectively, to transition metals.

Insight of frontier molecular orbital's of HOMO, LUMO, and UV-VIS

The lowest unoccupied molecular orbital (LUMO) energy is generated by ionization, and the highest occupied molecular orbital (HOMO) energy is observed by the electron affinity. These parameters have been evaluated for adsorption of carbon dioxide and nitrogen dioxide on the (Fe, Ni, Zn) and (Mn, Co, Cu), respectively, doping of nanographene as the gas detector in Table 5. The HOMO (au), LUMO (au), and band energy gap ($\Delta E = E_{LUMO} - E_{HOMO}$) (ev) have exhibited the pictorial explanation of the frontier molecular orbitals and their respective positive and negative areas which are a significant parameter for discovering the molecular properties of efficient compounds in adsorption of CO_2 and NO_2 on the TM-doped nanographene surface. (Table 5).

Moreover, for getting more conclusive approving in identifying the compound characteristics of adsorption complexes of CO_2 on the (Fe, Ni, Zn) and NO_2 on the (Mn, Co, Cu), respectively, doping of C-nanographene surfaces, a series of chemical reactivity parameters such as chemical potential (μ), electronegativity (χ), hardness (η), softness (ζ), and electrophilicity index (ψ) has been carried out (Table 5) [46–48].

Figure 7 shows the chemical potential (μ) for CO_2 and NO_2 adsorption on the (Fe, Ni, Zn) and (Mn, Co, Cu), respectively, doping of C-NG surfaces. However, CO_2 adsorption on the surface of zinc doping of carbon-nanographene has a considerable minimum potential well. The negative content of the chemical potential (μ) and the positive contents of other factors have remarked an admissible efficiency of scavenging CO_2 by zinc-doped carbon-nanographene. In fact, the chemical potential defined the increase of CO_2 molecules to the crystal of Zn@C-NG, while the number of other particles and the number of unoccupied lattice locations keep constant. As a matter of fact, enhancement of the gas molecules of CO_2 thus involves the simultaneous increasing a lattice site or unit cell to the crystal of Zn@C-NG surface. This procedure heads to an augment in surface region and, thereby, energy must be spent in generating a new surface of nanographene. In addition, the alliance of particle alters the mass of the crystal and process is also accomplished versus the mechanical powers.

Table 5 Doping of nanographene as the gas detector

Gas→ TM@C-NG	LUMO	HOMO	ΔE	μ	χ	η	ζ	ψ
:Ö = C = Ö: → Fe@ C-NG	-0.0070	-0.1234	3.1666	-1.7748	1.7748	1.5833	0.3158	0.9947
:Ö = C = Ö: → Ni @ C-NG	-0.0049	-0.1389	3.6471	-1.9563	1.9563	1.8235	0.2742	1.0494
:Ö = C = Ö: → Zn@ C-NG	-0.0973	-0.2735	4.7952	-5.0463	5.0463	2.3976	0.2085	5.3105
:Ö:−Ṅ = Ö: → Mn@ C-NG		-0.1479	3.7853	-2.1335	2.1335	1.8927	0.2641	1.2024
:Ö:−Ṅ = Ö: → Co@ C-NG	-0.0077	-0.1570	4.0621	-2.2419	2.2419	2.0310	0.2462	1.2373
:Ö:−Ṅ = Ö: → Cu@ C-NG	-0.0115	-0.1596	4.0302	-2.3280	2.3280	2.0151	0.2481	1.3447

$\Delta E = E_{LUMO}\text{-}E_{HOMO}$; $\mu = (E_{HOMO} + E_{LUMO})/2$; $\chi = -(E_{HOMO} + E_{LUMO})/2$; $\eta = (E_{LUMO} - E_{HOMO})/2$; $\zeta = 1/(2\eta)$; $\psi = \mu^2/(2\eta)$

In this work, energy gap establishes how toxic gases of CO_2 and NO_2 can be adsorbed on the (Fe, Ni, Zn) and (Mn, Co, Cu), respectively, doping of nanographene as the gas sensors at B3LYP/LANL2DZ, 6-311 + G (2d, p) quantum approach. In addition, frontier molecular orbitals perform an essential function in the optical and electrical factors like ultraviolet and visible spectrums [49].

The energy gap between LUMO and HOMO has recognized the qualifications of molecular electrical transport [50]. Through Frank-Condon formula, the most value of absorption peak (max) is related to an ultraviolet and visible spectrum to vertical stimulation.

Furthermore, TD-DFT/ LANL2DZ, 6-31 + G (d,p) calculations have been accomplished to discern the low-lying excited states of CO_2 and NO_2 adsorbed on the (Fe, Ni, Zn) and (Mn, Co, Cu), respectively, doping of nanographene. The consequences contain the vertical stimulation energies, oscillator strength, and wavelength which have been introduced in Fig. 8a–f.

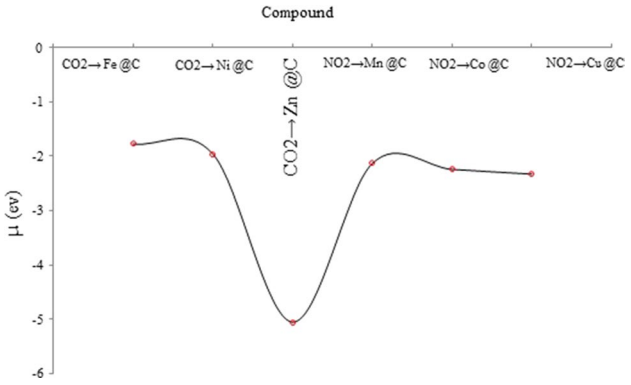

Fig. 7 The chemical potential (μ) for CO_2 and NO_2 adsorption on the (Fe, Ni, Zn) and (Mn, Co, Cu), respectively

Figure 8 a–f shows the UV-VIS spectrums for $CO_2 \rightarrow$ Fe @C-NG, $CO_2 \rightarrow$ Ni @C-NG, and $CO_2 \rightarrow$ Zn @C-NG and $NO_2 \rightarrow$ Mn @C-NG, $NO_2 \rightarrow$ Co @ C-NG, and $NO_2 \rightarrow$ Cu @C-NG, respectively, with maximum adsorption bands between 1000 and 5000 nm. Moreover, it has been observed a sharp peak around 2500 nm for $CO_2 \rightarrow$ TM@C-NG and $NO_2 \rightarrow$ TM@C-NG surfaces (Fig. 8a–f).

Conclusion

This research aimed to remark the study of polluting gas of carbon dioxide and nitrogen dioxide adsorption employing graphene nanosheet. The graphene sheet reviewed in general physically adsorb many of the pollutant gas molecules considered, and the interaction can usually enhance by transition metal doping which ameliorate their detecting properties through chemisorption study.

This article has reported the trends for environmental pollutant gases of carbon dioxide (CO_2) and nitrogen dioxide (NO_2) chemisorption on transition metals of (iron, nickel, zinc) and (manganese, cobalt, copper), respectively, doping of carbon-nanographene surface.

In particular, the energetic, structural, and infrared adsorption characteristics of linearly (atop) CO_2 and NO_2 adsorbed on (Fe, Ni, Zn) and (Mn, Co, Cu), respectively, doping of C-NG have been discussed. Spin-unrestricted density functional theory (DFT) calculations were applied to verdict the tendency of CO_2 and NO_2 adsorption energy of ($CO_2 \rightarrow$ Fe, $CO_2 \rightarrow$ Ni, $CO_2 \rightarrow$ Zn) and ($NO_2 \rightarrow$ Mn, $NO_2 \rightarrow$Co, $NO_2 \rightarrow$Cu) doped on the nanographene sheet and normal mode vibrational frequencies (ν_{CO2} and ν_{NO2})

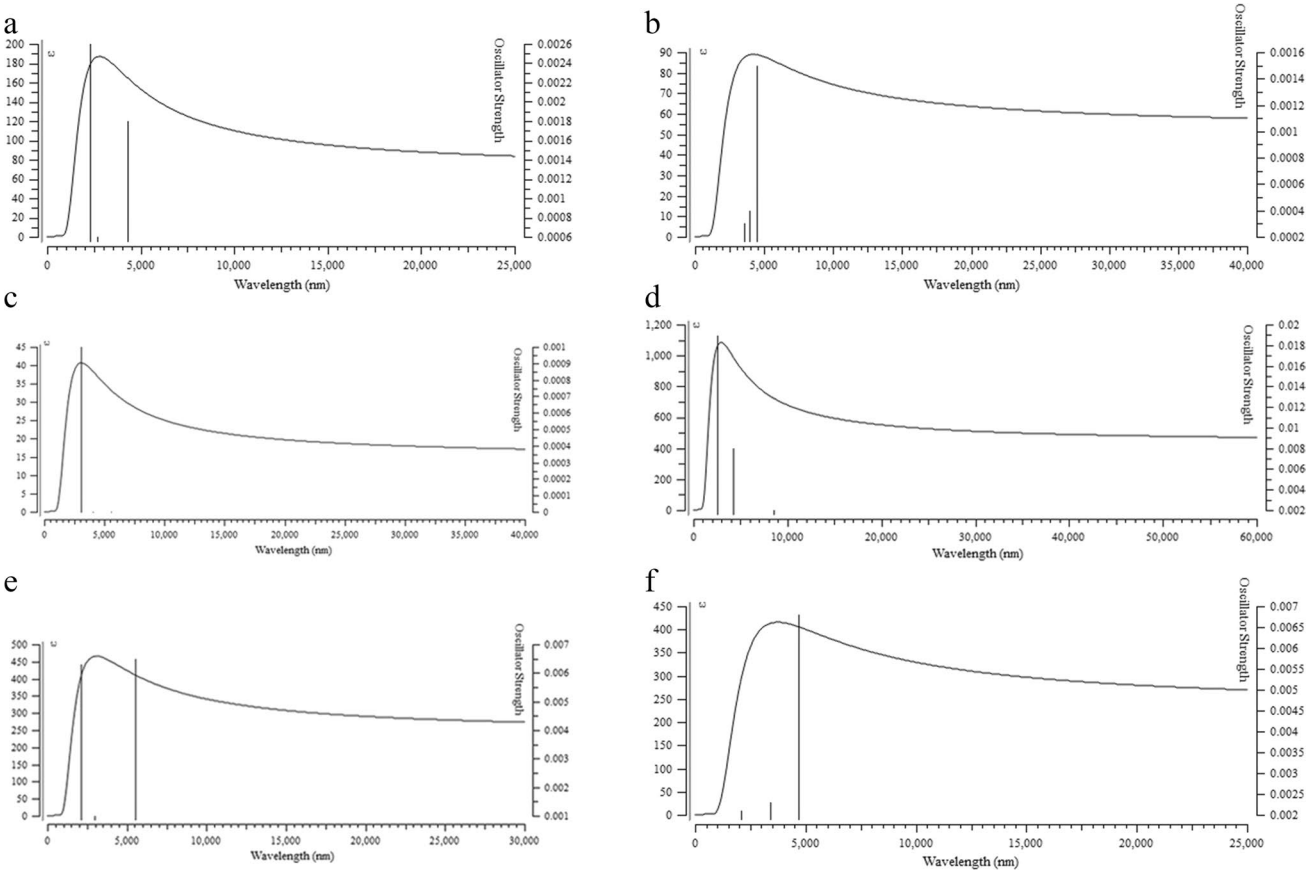

Fig. 8 The consequences of the TD-DFT/ LANL2DZ, 6-31 + G (d,p) calculations contain the vertical stimulation energies, oscillator strength, and wavelength

of : Ö = C = Ö : and : Ö : –Ṅ = Ö : for clusters composed of Fe, Ni, and Zn and Mn, Co, and Cu, respectively.

The effects of the transition metal electronic structure onto the adsorption energy of CO_2 and NO_2 toxic gases and how these chemical factors might be related to the catalytic activity of transition supported metal catalysts that deal with the adsorption, and surface diffusion, have been investigated.

Acknowledgements In successfully completing this paper and its research, the authors are grateful to Kastamonu University for their support through the library, the laboratory, and scientific websites.

Author contribution Fatemeh Mollaamin: conceptualization and idea, methodology, software, validation, formal analysis, investigation, data curation, writing—original draft preparation, visualization, supervision, project administration. Majid Monajjemi: methodology, software, formal analysis, investigation, data curation, writing—review and editing, visualization, resources.

Data availability It is not applicable.

Declarations

Ethics approval The authors consent to participate and publish the data.

Competing interests The authors declare no competing interests.

References

1. Su Y, Wang J, Wang B, Yang T, Yang B, Xie G, Zhou Y, Zhang S, Tai H, Cai Z et al (2020) Alveolus-inspired active membrane sensors for self-powered wearable chemical sensing and breath analysis. ACS Nano 14:6067–6075. https://doi.org/10.1021/acsnano.0c01804
2. Ma D, Zhang J, Li X, He C, Lu Z, Lu Z, Lu Z, Yang Z, Wang Y (2018) C3N monolayers as promising candidates for NO2 sensors. Sens Actuators B Chem 266:664–673. https://doi.org/10.1016/j.snb.2018.03.159
3. Pacheco M, Pacheco J, Valdivia R, Santana A, Tu X, Mendoza D, Frias H, Medina L, Macias J (2017) Green applications of carbon nanostructures produced by plasma techniques. MRS Adv 2:2647–2659
4. Kroto HW, Heath JR, O'Brien SC, Curl RF, Smalley RE (1985) C60: Buckminsterfullerene. Nature 318:162–163
5. Nasibulin AG, Pikhitsa PV, Jiang H, Brown DP, Krasheninnikov AV, Anisimov AS, Queipo P, Moisala A, Gonzalez D, Lientschnig G et al (2007) A novel hybrid carbon material. Nat Nanotechnol 2:156–161
6. Moisala A, Nasibulin AG, Shandakov SD, Jiang H, Kauppinen EI (2005) On-line detection of single-walled carbon nanotube formation during aerosol synthesis methods. Carbon 43:2066–2074
7. Delgado JL, Herranz M, Martín N (2008) The nano-forms of carbon. J Mater Chem 18:1417
8. Falcao EH, Wudl F (2007) Carbon allotropes: beyond graphite and diamond. J Chem Technol Biotechnol 82:524–531
9. Langenhorst F, Campione M (2019) Ideal and real structures of different forms of carbon, with some remarks on their geological significance. J Geol Soc 176:337–347
10. Louis H, Patrick M, Amodu IO, Benjamin I, Ikot IJ, Iniama GE, Adeyink AS (2023) Sensor behavior of transition-metals (X = Ag, Au, Pd, and Pt) doped Zn11-X-O12 nanostructured materials for the detection of serotonin. Mater Today Commun 34:105048. https://doi.org/10.1016/j.mtcomm.2022.105048
11. Odey DO, Edet HO, Louis H, Gber TE, Nwagu AD, Adalikwu SA, Adeyinka AS (2023) Heteroatoms (B, N, and P) doped on nickel-doped graphene for phosgene ($COCl_2$) adsorption: insight from theoretical calculations. Mater Today Sustain 21:100294. https://doi.org/10.1016/j.mtsust.2022.100294
12. Louis H, Charlie DE, Amodu IO, Benjamin I, Gber TE, Agwamba EC, Adeyinka AS (2022) Probing the reactions of thiourea (CH4N2S) with metals (X = Au, Hf, Hg, Ir, Os, W, Pt, and Re) anchored on fullerene surfaces (C59X). ACS Omega 7(39):35118–35135. https://doi.org/10.1021/acsomega.2c04044
13. Lee SW, Lee W, Hong Y, Lee G, Yoon DS (2018) Recent advances in carbon material-based NO_2 gas sensors. Sens Actuators B Chem 255:1788–1804. https://doi.org/10.1016/j.snb.2017.08.203
14. Chatterjee SG, Chatterjee S, Ray AK, Chakraborty AK (221) Graphene–metal oxide nanohybrids for toxic gas sensor: A review. Sens Actuators B Chem:1170–1181
15. Xiao Z, Kong LB, Ruan S, Li X, Yu S, Li X, Jiang Y, Yao Z, Ye S, Wang C et al (2018) Recent development in nanocarbon materials for gas sensor applications. Sens Actuators B Chem 274:235–267. https://doi.org/10.1016/j.snb.2018.07.040
16. Monajjemi M, Baie MT, Mollaamin F (2010) Interaction between threonine and cadmium cation in [Cd(Thr)] (n = 1–3) complexes: density functional calculations. *Russ Chem Bull 59*:886–889
17. Khalili Hadad B, Mollaamin F, Monajjemi M (2011) Biophysical chemistry of macrocycles for drug delivery: A theoretical study. *Russ Chem Bull 60*:238–241
18. Monajjemi M, Khaleghian M, Tadayonpour N, Mollaamin F (2010) The effect of different solvents and temperatures on stability of single-walled carbon nanotube: A QM/MD study. *Int J Nanosci 09*:517–529
19. Bakhshi K, Mollaamin F, Monajjemi M (2011) Exchange and correlation effect of hydrogen chemisorption on nano V(100) surface: a DFT study by generalized gradient approximation (GGA). *J Comput Theor Nanosci 8*:763–768. https://doi.org/10.1166/jctn.2011.1750
20. Mollaamin F, Ilkhani A, Sakhaei N, Bonsakhteh B, Faridchehr A, Tohidi S, Monajjemi M (2015) Thermodynamic and solvent effect on dynamic structures of nano bilayer-cell membrane: hydrogen bonding study. *J Comput Theor Nanosci 12*:3148–3154. https://doi.org/10.1166/jctn.2015.4092
21. Adanna D, Nwagu AD, Louis H, Edet HO, Benjamin I, Osabor VN, Adeyinka AS (2023) Computational study on nickel doped encapsulated Mg, K, Ca on pristine C24 nanocage for gas sensing applications. Mater Sci Semicond Process 157:107334. https://doi.org/10.1016/j.mssp.2023.107334
22. Mohammadi MD, Abbas F, Louis H, Mathias GE, Unimuke TO (2022) Trapping of CO, CO2, H2S, NH3, NO, NO2, and SO2 by polyoxometalate compound. Comput Theor Chem 1215:113826. https://doi.org/10.1016/j.comptc.2022.113826
23. Louis H, Egemonye TGC, Unimuke TO, Inah BE, Edet HO, Eno EA, Adalikwu SA, Adeyinka AS (2022) Detection of carbon, sulfur, and nitrogen dioxide pollutants with a 2D $Ca_{12}O_{12}$ nanostructured Material. ACS Omega 7(39):34929–34943. https://doi.org/10.1021/acsomega.2c03512
24. Louis H, Amodu IO, Unimuke TO, Gber TE, Isang BB, Adeyinka AS (2022) Modeling of $Ca_{12}O_{12}$, $Mg_{12}O_{12}$, and $Al_{12}N_{12}$ nanostructured materials as sensors for phosgene (Cl2CO). Mater Today Commun 32:103946. https://doi.org/10.1016/j.mtcomm.2022.103946
25. Mollaamin F, Monajjemi M (2022) Molecular modelling framework of metal-organic clusters for conserving surfaces: Langmuir sorption through the TD-DFT/ONIOM approach. *Mol Simul 49*:365–376. https://doi.org/10.1080/08927022.2022.2159996
26. Mollaamin F, Shahriari S, Monajjemi M, Khalaj Z (2022) Nanocluster of aluminum lattice via organic inhibitors coating: a study

of Freundlich adsorption. J Clust Sci:1–16. https://doi.org/10.1007/s10876-022-02335-1
27. Hanaor DAH, Ghadiri M, Chrzanowski W, Gan Y (2014) Scalable surface area characterization by electrokinetic analysis of complex anion adsorption (PDF). Langmuir 30(50):15143–15152. https://doi.org/10.1021/la503581e
28. Boyd A, Dube I, Fedorov G, Paranjape M, Barbara P (2014) Gas sensing mechanism of carbon nanotubes: from single tubes to high-density networks. Carbon 69:417–423
29. Zhao J, Buldum A, Han J, Lu JP (2002) Gas molecule adsorption in carbon nanotubes and nanotube bundles. Nanotechnology 13:195–200
30. Svensson M, Humbel S, Froese RDJ, Matsubara T, Sieber S, Morokuma K (1996) ONIOM: A multilayered integrated MO + MM method for geometry optimizations and single point energy predictions. A test for Diels−Alder reactions and Pt(P(t-Bu)3)2 + H2 oxidative addition. J Phys Chem 100(50):19357–19363. https://doi.org/10.1021/jp962071j
31. Brandt F, Jacob CR (2022) Systematic QM region construction in QM/MM calculations based on uncertainty quantification. J Chem Theory Comput *18*(4):2584–2596. https://doi.org/10.1021/acs.jctc.1c01093
32. Becke AD (1993) Density-functional thermochemistry. III. The role of exact exchange. J Chem Phys 98:5648–5652
33. Lee C, Yang W, Parr RG (1988) Development of the Colle–Salvetti correlation-energy formula into a functional of the electron density. Phys Rev B 37:785–789
34. Grimme S, Antony J, Ehrlich S, Krieg H (2010). J Chem Phys 132:154104. https://doi.org/10.1063/1.3382344
35. Grimme S, Antony J, Ehrlich S, Krieg H (2010) A consistent and accurate ab initio parametrization of density functional dispersion correction (DFT-D) for the 94 elements H-Pu. J Chem Phys 132:154104. https://doi.org/10.1063/1.3382344
36. Becke AD (1988) Density-functional exchange-energy approximation with correct asymptotic behavior. *Phys Rev A 38*:3098–3100
37. Ditchfield R, Hehre WJ, Pople JA (1971) Self-consistent molecular-orbital methods. IX. An extended Gaussian-type basis for molecular-orbital studies of organic molecules. *J Chem Phys. 54*:724–728
38. Frisch MJ, Trucks GW, Schlegel HB, Scuseria GE, Robb MA, Cheeseman JR, Scalmani G, Barone V, Petersson GA, Nakatsuji H, Li X, Caricato M, Marenich AV, Bloino J, Janesko BG, Gomperts R, Mennucci B, Hratchian HP, Ortiz JV et al (2016) Gaussian 16, Revision C.01. Gaussian, Inc., Wallingford CT
39. Fry RA, Kwon KD, Komarneni S, Kubicki JD, Mueller KT (2006) Solid-state NMR and computational chemistry study of mononucleotides adsorbed to alumina. Langmuir 22:9281–9286
40. Smith JAS (1971) Nuclear quadrupole resonance spectroscopy. J Chem Educ 48:39–41
41. Garroway AN (2003) Appendix K: Nuclear quadrupole resonance, by, Naval Research Laboratory. In: Jacqueline MacDonald JR (ed) Lockwood: Alternatives for landmine detection. Report MR-1608. Rand Corporation
42. Poleshchuck OK, Kalinna EL, Latosinska JN, Koput J (2001). J Mol Struct Theochem 547:233–243
43. Young HA, Freedman RD (2012) Sears and Zemansky's University Physics with Modern Physics13th edn. Addison-Wesley, Boston, p 754
44. Cortés-Arriagada D, Villegas-Escobar N, Ortega DE (2018) Fe-doped graphene nanosheet as an adsorption platform of harmful gas molecules (CO, CO_2, SO_2 and H2S), and the co-adsorption in O2 environments. Appl Surf Sci 427, Part B:227–236. https://doi.org/10.1016/j.apsusc.2017.08.216
45. Tahan A, Mollaamin F, Monajjemi M (2009) Thermochemistry and NBO analysis of peptide bond: Investigation of basis sets and binding energy. *Russ J Phys Chem A 83*:587–597. https://doi.org/10.1134/S003602440904013X
46. Kohn W, Becke AD, Parr RG (1996) Density functional theory of electronic structure. *J Phys Chem 100*:12974–12980. https://doi.org/10.1021/jp960669l
47. Parr RG, Pearson RG (1983) Absolute hardness: companion parameter to absolute electronegativity. *J Am Chem Soc. 105*:7512–7516. https://doi.org/10.1021/ja00364a005
48. Politzer P, Abu–Awwad FA (1998) Comparative analysis of Hartree-Fock and Kohn-Sham orbital energies. *Theor Chem Acc 99*:83–87. https://doi.org/10.1007/s002140050307
49. Aihara J (1999) Reduced HOMO−LUMO gap as an index of kinetic stability for polycyclic aromatic hydrocarbons. J Phys Chem A 103(37):7487–7495. https://doi.org/10.1021/jp990092i
50. Silverstein RM, Bassler GC, Morrill TC (1981) Spectrometric identification of organic compounds5th edn. John Wiley & Sons, Inc., New York